Detection of poloidally symmetric, radially localized, random flow structures in tokamak plasma (KFKI RMKI-REPORT)

A. Bencze, M. Berta, S. Zoletnik

2005

Abstract

This report presents the first application of the autocorrelation technique[1] to detect and characterize the microturbulence-zonal flow system using fluctuating signals ($\tilde{\phi}_f, \tilde{I}_s$) measured by special arrays of Langmuir probes in the Castor tokamak. Radially localized ($\approx 1cm$) random flow structures has been clearly observed with a lifetime of $\approx 1ms$ and long-range (measurements have been extended up to $12cm$ poloidal distance) poloidal correlation (m=0). Linkage between flow variation and the local density profile has also been demonstrated.

Contents

Chapter 1

What zonal flows are?

Nowadays it is generally accepted by the fusion community that the understanding of the drift wave - zonal flow turbulence plays a crucial role in the understanding and handling of anomalous transport and different spontaneous transitions of the collective plasma state.

From theoretical point of view drift wave (DW) turbulence consists of unstable potential modes $(\mathbf{k}, \omega)$, with $k_{\|} \ll k_{\perp} \gg 1/L_{\perp}$, and $\omega \ll \Omega_{ci}$, where $(\|, \perp)$ denote directions with respect to the confining magnetic field, $L_{\perp}$ is the perpendicular macroscopic size of the system and $\Omega_{ci} = eB/m_i$ is the ion cyclotron frequency. The free energy sources of DW instability are the gradients of macroscopic profiles (density, temperature etc.). The 'equilibrium' spectrum of the fully developed DW turbulence can be unstable in the presence of random shear flows or zonal flows which are potential modes with $(k_r, k_\theta, k_\phi) = (k_r, 0, 0)$. The effect of shearing can be described as a diffusion of the DW radial wave number in $\mathbf{k}$-space. In order to conserve drift wave action density, the increase of DW radial wave number causes a decrease in DW energy and as the energy of the zonal flow-drift wave system must be conserved a zonal flow growth will arise. It has to be noted that the excitation of ZF modes - mediated by the radial gradient of the DW turbulent Reynolds stress - is completely a nonlinear, nevertheless generic process in 2D turbulence named 'inverse cascade'. For comprehensive reviews in the topic of DW-ZF turbulence we refer the Reader to [2], [3].

The appearance of ZFs and its effect on regulating turbulent transport was first observed in numerical simulations at fluid, gyro-fluid and gyro-kinetic levels [4], [5], [6], [7].

First experimental investigations, which were devoted to the detection of sheard zonal flows and to clarify their connection to turbulence level and transport, followed the theory with a delay of almost a decade. It was shown by *Hidalgo et. al.* [8] that the electrostatic component of the Reynolds stress (R_s) has a significant gradient $(\mathrm{d}R_s/\mathrm{d}r \approx 10^7 - 10^8 m/s^2)$ close to the velocity shear layer location. Following this line at the HT-6M tokamak *Y.H. Xu* and his co-workers [9] measuring the time evolution of the turbulence-induced Reynolds stress gradient across the $L - H$ transition found strong correlation between the enhanced $\partial_r R_s$ and the poloidal flow acceleration. Recently the main terms entering in the momentum balance have been measured in an RFP configuration [10]. The complete Reynolds stress was found to be the main term opposing the action of the viscosity and then driving the shear of $\mathbf{E} \times \mathbf{B}$ velocity. The problem of flow generation can be reformulated as a three-wave mode-coupling problem [**?**], transforming the search for Reynolds stress profile changes into the study of the bispectrum of the potential fluctuations. Such nonlinear signal processing was done by *Moyer et. al.* [12] using turbulence data acquired in neutral beam heated discharges with spontaneous $L - H$ transitions in the DIII-D tokamak. The results shown transient increase in three-wave coupling between low and high frequencies just before and during the $L - H$ transition.

First indirect experimental identification of zonal flows using phase-contrast imaging of density fluctuations in the DIII-D tokamak, was done by *Coda and Porkolab* [13]. The BES measurements and the Time-Delay-Estimation analysis of *Jakubowski et. al.* [14] has been pointed to the existence of low

frequency ($\approx 15kHz$) nearly coherent oscillations in the poloidal flow. Such flows have been observed earlier in 3D Braginskii simulations [15] as a coherent branch of $(m = 0, n = 0)$ zonal flows named geodesic acoustic modes (GAM). The existance of GAM modes was also reported by *G. D. Conway et. al.* [16] at ASDEX by means of Doppler reflectometry. Last but not least we have to mention two recent experimental works on hunting random zonal flows. The first one has been performed at the HT-7 tokamak by *G. S. Xu* [**?**] and his co-workers using specially designed Langmuir probes, detecting floating potential fluctuations. Measuring $\tilde{E}_r$ with a poloidal separation of about 3 cm, they have found a separation in the coherency spectrum identifying the long life ambient turbulence peaking around $50KHz$, and a low frequency $< 10KHz$ radially localized mode. The second direct ZF identification in a stellarator (CHS) was very recentely done in [18] using toroidally separated($\approx 1.5m$) dual heavy ion beam probes.

Our present measurements aim at the identfication and detailed characterization of ZFs in tokamak plasmas. Autocorrelation technique has been used to extract information about the fluctuations in the flow velocity following the time evolution of the autocorrelation structure of the basic micro-turbulence. As it will be detailed below, properly defined quantity, named autocorrelaton-width ($W_{acf}(t)$) carries the informaton on the time modulation of $\tilde{\mathbf{E}}_r \times \mathbf{B}$ flow. The characteristic time scale of the random flow modulation has been deduced from the autocorrelation function (ACF) of $W_{acf}(t)$ while the radial and poloidal structure of the $W_{acf}(t)$ fluctuation have been extracted from the cross-correlation function (CCF) along a single rake and the CCF between the two rakes respectively.

Chapter 2

Experimental set-up

Fluctuation measurements have been done in the edge plasma of Ohmic-heated discharges in the CASTOR tokamak ($R = 0.4\,\mathrm{m}$, $a = 8.5\,\mathrm{cm}$, $B_t \leq 1.5\,\mathrm{T}$, $I_p \leq 25\,\mathrm{kA}$, $T_{shot} \leq 50\,\mathrm{ms}$, $n_e = (0.2 - 0.3) \cdot 10^{19}\,\mathrm{m}^{-3}$, $T_e(0) \sim 200\,\mathrm{eV}$), using two *rake probes*, as shown in Figure 2.1.

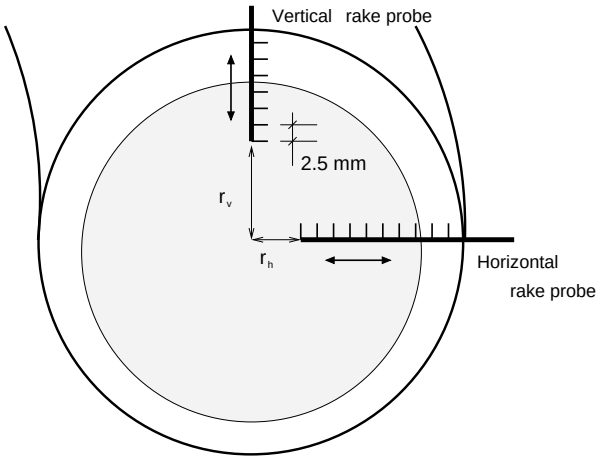

Figure 2.1: The experimental set-up

Each rake probe consists of an array of Langmuir-probe tips spaced by $2.5mm$. Every odd tip has been operated in *floating potential* regime , while each even probe has been operated in *ion saturation current* regime. If we assume as usual that the temperature fluctuations are negligible, using the tip-arrangement decribed above, we are able to measure at the same radial position the radial electric field fluctuations and the density fluctuations. (Toroidal angle between the plane of experiment and plane of limiter was 135^o, and radius of limiter diafragma was 85 mm.)

Figure 2.2: Picture of the radial rake probe

Chapter 3

Signal processing

In the course of our experimental campagne standard shots have been made with main parameters shown in Table 3.1 where it is also idicated the radial position of the vertical and horizontal rake probe with respect to the tokamak center. For data analysis we have selected a time interval of $15ms$ length in the stationary phase of the discharges (global plasma parameters are seen in Fig. 3.1).

Shots	r_V [mm]	r_H [mm]	I_p [kA]	B_T [T]	Comments
20511-20531	70	77	8	1.3	-

Table 3.1: Characterization of the investigated shot–series

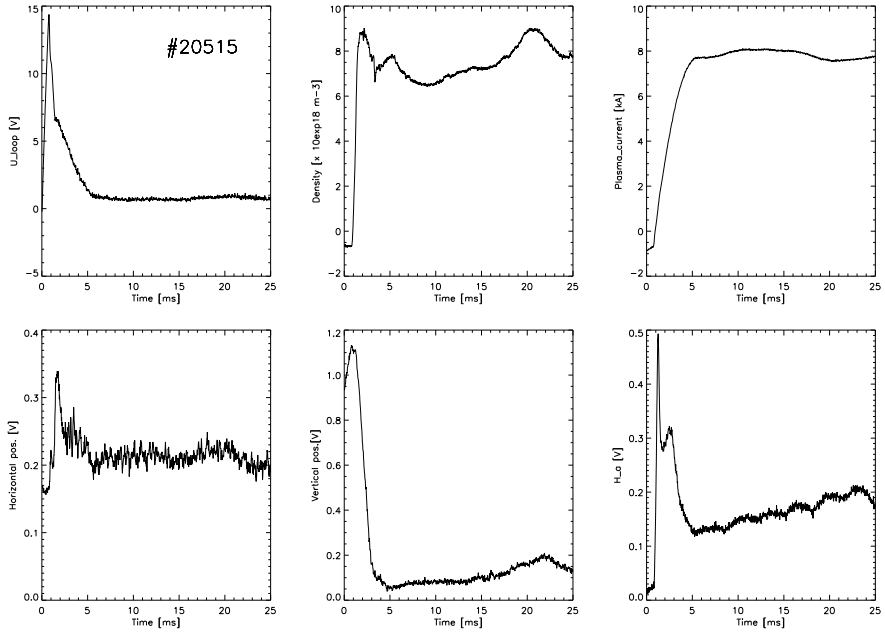

Figure 3.1: Main plasma parameters in # 20515.

In order to improve statistics, we have used an ensemble of 20 shots which are though to be 'identical' in a given statistical sens. That means that we have calculated the first four moments of the fluctuating signal for each shot belonging to the ensemble. Table 3.2 shows the average value and its uncertenty of the moments for shots in Table 3.1.

Standard deviation	Kurtosis	Skewness
0.0102 ± 0.0017	3.363 ± 0.176	-0.0059 ± 0.001

Table 3.2: Statistical identity of shots in Table 3.1.

3.1 Autocorrelation technique

In this section we investigate the possibility of detecting B-perpendicular flow modulations through observing temporal variations of the autocorrelation function (ACF) in a single-point measurement of plasma turbulence. In order to calculate the sensitivity of the method we found it essential to analyse the statistical scatter of the autocorrelation function due to two effects: the finite number of turbulent eddies and/or detector statistical noise. The final result of this derivation is a simple expression readily usable to various measurements. Details of the derivation can be found in [1]

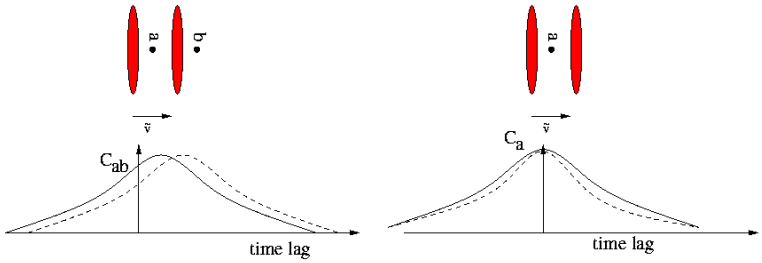

Figure 3.2: Sketch of one-point (left) and two-point (right) measurement

Investigating correlation functions we can get information about statistical properties of turbulent structures: the correlation time, the correlation length along a spatial coordinate and the propagation velocity from cross-correlation function. From a very simple model, which deals with poloidally moving structures having Gaussian shape both in space and time, we can calculate the autocorrelations time in a single-point measurement as a function of the eddy lifetime τ_{life} and the velocity dependent propagation time τ_v:

$$w_t = \frac{\tau_{life} \cdot \tau_v}{\sqrt{\tau_{life}^2 + \tau_v^2}} \tag{3.1}$$

where $\tau_v = w_\phi / v_\phi$, w_ϕ is the poloidal correlation length and v_ϕ is the poloidal flow velocity. From this formula it is clear that we have two distinct limiting cases:

- $\tau_{life} \gg \tau_v$:for a fixed w_ϕ spatial correlation length the correlation time w_t depends mainly on v_ϕ; $w_t \approx w_\phi / v_\phi$. In this case from the correlation time we can follow the time evolution of the $v_\phi(t)$ flow velocity.

- $\tau_{life} \ll \tau_v$:in this case the correlation time gives information about the eddy lifetime and the flow velocity cannot be deduced.

The heart of the autocorrelation method lies in the validity of the first assumption. In this case the procedure is the following: first we split the whole time record in shorter ΔT intervals, where the $\Delta T \gg w_t$ relation must hold. Than we calculate autocorrelation functions from these short time intervals and extract the information about the width of the autocorrelation function. In this way we obtain the ACF-width (denoted by $W_{acf}(t)$) as a function of time with time resolution determined by ΔT. After

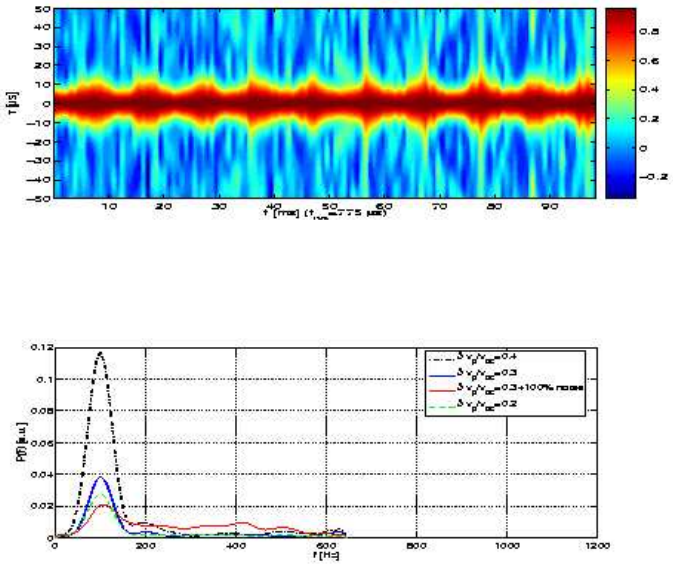

Figure 3.3: Illustration of method (more details see in the text)

this procedure we are ready to analyse $W_{acf}(t)$ using correlation technique or spectral methods. It has to be noted that $W_{acf}(t)$ can be defined in different ways. In this work, as will be described later, W_{acf} has been taken to be the first moment of the autocorrelation function.

To illustrate the feasibility of the method 1+1 dimensional simulation was done. Identical Gaussian pulses were moved across a single detection channel with a variable flow velocity. The lifetime (τ_{life}) of these events was much longer than their transit time over the observation volume (τ_v) and the pulses were always generated before reaching the observation. The flow velocity was modulated sinusoidally. In some cases an additional Gaussian noise was added to the signal simulated with time resolution of $1\mu s$.

The autocorrelation function was calculated for short time intervals. The effect of the 100Hz velocity modulation applied in this simulation is clearly observable in Fig. 3.3. The power spectrum of the autocorrelation-width signal is shown in Fig. 3.3. (bottom) for different velocity modulation amplitudes from 0.2 to 0.4. The peak at 100Hz clearly shows up in all cases. In one of the plotted cases an additional normally distributed random noise was added with an RMS amplitude identical to the RMS amplitude of the original signal. The resulting power spectrum exhibits a broadband noise and somewhat reduced sensitivity to the 100 Hz modulation, but the peak is clearly distinguishable.

3.1.1 Statistics of the autocorrelation function

In order to evaluate the sensitivity of the method above, an analytical expression was derived [1] for the relative scatter of the autocorrelation function. In our calculation we assume that we have a measured time signal which consist of randomly distributed, limited temporal length events, including overlapping as well. Each event has a time evolution and it is described by a set of random variables (with a given but otherwise arbitrary distribution function) such as the amplitude, the lifetime, the time center etc. Starting from the standard definitions of the autocorrelation function and statistical variance and introducing different kind of statistical averaging, it is possible to derive a formal expression for the relative scatter of the autocorrelation function. Using some reasonable assumptions such as the large number of events

($N_s \gg 1$) and long integration time relative to the average correlation time ($w_t/\Delta T \ll 1$), we can deduce the following tendency:

$$\frac{\sigma}{\langle C_a \rangle} = D \cdot \sqrt{\frac{w_t}{\Delta T}} \tag{3.2}$$

where σ is the standard deviation of the autocorrelation function $\langle C_a \rangle$ denotes the average autocorrelation function at zero time lag, and D is a constant depending on the details of the distributions of different random variables describing turbulent events. In case of events with uniform Gaussian shape the value of D can be easily calculated and has been found to be $D = (2\pi)^{1/4}$.

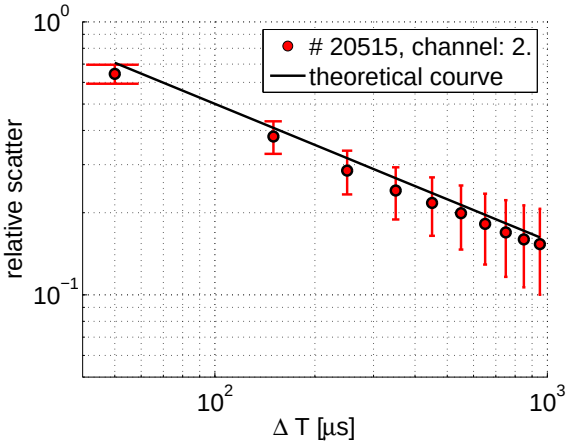

Figure 3.4: Gaussian theory vs. experimental data from fluctuation measurements

The results of this simple model are compared with real fluctuation measurements (see. Fig. 3.4.) done at the Castor tokamak by means of Langmuir probes operating in ion saturation current regime.

3.1.2 Sensitivity of the method

In this section the response of the properely defined ACF-width function to the small modulations in the autocorrelation time w_t has been investigated. We define the measure of the autocorrelation width as:

$$W_{acf}(w_t(t)) = \int_0^\infty \tau \cdot C_a\left(\tau; w_t(t)\right) \mathrm{d}\tau. \tag{3.3}$$

In the following we assume that the shape of the autocorrelation function is $\exp\left(-\frac{\tau^2}{2w_t^2(t)}\right)$. This assumption in our case is supported by measurements(see Fig. 3.4). In our limiting case the autocorrelation time $w_t(t) = w_\phi/v_\phi(t)$ depends on the poloidal flow velocity. Now we split $w_t(t)$ in two parts:

$$w_t(t) = w_t^0 + \delta w_t(t). \tag{3.4}$$

As we would like to determine modulations in the ACF-width ($W_{acf}(t)$) originating from flow variation, using Eq. (3.3), a natural question is arised: what is the relation between correlation time variation (or poloidal velocity variation) and variatons in $W(t)$? In order to answer this question we expand C_a around w_t^0, assuming $\epsilon = \frac{\delta w_t}{w_t^0} \ll 1$.

$$C_a \quad = \quad C_a|_{\epsilon=0} + \left.\frac{\partial C_a}{\partial \epsilon}\right|_{\epsilon=0} \cdot \epsilon + \mathcal{O}\left(\epsilon^2\right) \tag{3.5}$$

$$\frac{\partial C_a}{\partial \epsilon} = \exp\left\{-\frac{\tau^2}{2w_t^{0\,2}(1+\epsilon)^2}\right\}\cdot\left(-\frac{\tau^2}{2w_t^{0\,2}}\right)\cdot\frac{\partial}{\partial\epsilon}(1+\epsilon)^{-2}$$
$$\overset{\epsilon=0}{=} \exp\left\{-\frac{\tau^2}{2w_t^{0\,2}}\right\}\cdot\left(\frac{\tau^2}{w_t^{0\,2}}\right), \tag{3.6}$$

collecting all terms we arrive to

$$C_a = C_a^0 + C_a^0\cdot\left(\frac{\tau^2}{w_t^{0\,2}}\right)\cdot\left(\frac{\delta w_t}{w_t^0}\right) + \mathcal{O}\left[\left(\frac{\delta w_t}{w_t^0}\right)^2\right]. \tag{3.7}$$

Let us return to the original definition in Eq. (3.3) and using the known formula $\int_0^\infty x^n e^{-ax^2}\mathrm{d}x = \frac{\Gamma\left(\frac{n+1}{2}\right)}{2a^{\frac{n+1}{2}}}$, where $a>0, n>-1$ and $\Gamma(x)$ is the gamma function, the generalization of factorials.

$$W_{acf} = \int_0^\infty \tau\cdot C_a^0(\tau)\,\mathrm{d}\tau + \frac{\delta w_t}{w_t^0}\int_0^\infty\left(\frac{1}{w_t^0}\right)^2\tau^3\cdot C_a^0(\tau)\,\mathrm{d}\tau = W_0 + W_1. \tag{3.8}$$

Evaluating integrals W_0 and W_1 using properties of gamma function $\Gamma(1)=\Gamma(2)=1$, we obtain:

$$\frac{W_{acf}-W_0}{W_0} = 2\frac{\delta w_t}{w_t^0}. \tag{3.9}$$

We can conclude that defining ACF-width as it has been done in Eq. (3.3), in the framework of our model modulations in the flow can be amplified by a factor of two. Of course in a real experimental data processing, the integration limit canot be extended to infinity, but to finite τ_0. In this case the sensitivity of the method decreases as it can be seen in Fig. 3.5.

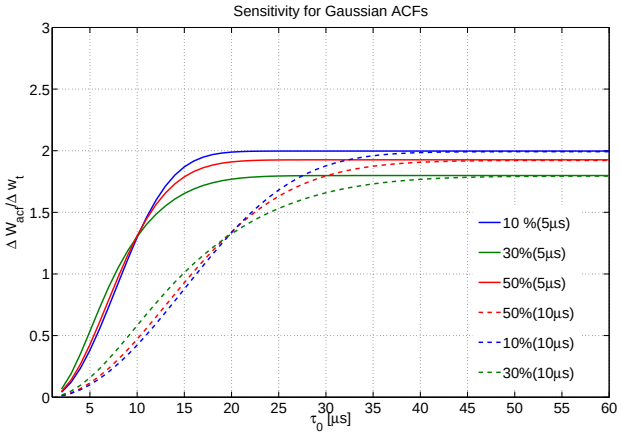

Figure 3.5: Dependence of the amplification factor on integration limit τ_0 at two different correlation times. Note, that henceforth in this papper we will use two times larger value for the autocorrelation time due to the symmetry of ACF, so our case is indicated in this figure by solid lines ($5\mu s$) at three different velocity modulations.

Chapter 4

Results

4.1 Time-scale separation

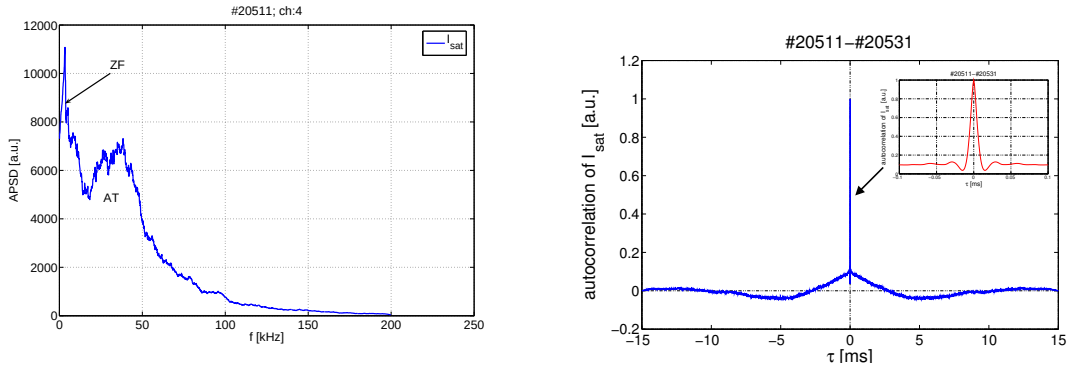

Figure 4.1: Power density spectrum (left) and autocorrelation (right) of local density fluctuations

Two distinct time scales can be observed in Fig. 4.1.On the one hand the basic micro-turbulence, characterized by $30 - 40kHz$ fluctuations has been ivestigated using spectrally filtered signals as seen in the left plot of Fig. 4.2. On the other hand a pronounced peak is present at lower frequencies wich can be linked with plasma flow modulations as it will be shown later in this report.

4.2 Characterization of the basic micro-turbulence

In the previous chapter it has been pointed out that the autocorrelation technique can be used in the cases when the poloidal flow velocity dominates the autocorrelation time of the basic turbulent structures. In order to check this statement previous measurements has been done in the Castor tokamak (during the summer course 2003) using two poloidally separated Langmuir probes. Autocorrelation function (left) and cross-correlation function (rigth) of the density fluctuations are seen in Fig. 4.3. The radial electric field has been risen applying edge biasing wich also results in the enhacement of the poloidal rotation (see the dashed courve in the Fig. 4.3).

The plots in the Fig. 4.3 clearly show roughly two times larger shift of the maximum of CCF (rigth hand side plot,red line)in the no-biased case – indicating two times lower velocity –, and two times wider ACF-width (left hand side plot,red line) indicating that our measurements lie in the region, where $\tau_{life} \gg \tau_v$ so the ACF-width method can be applied.

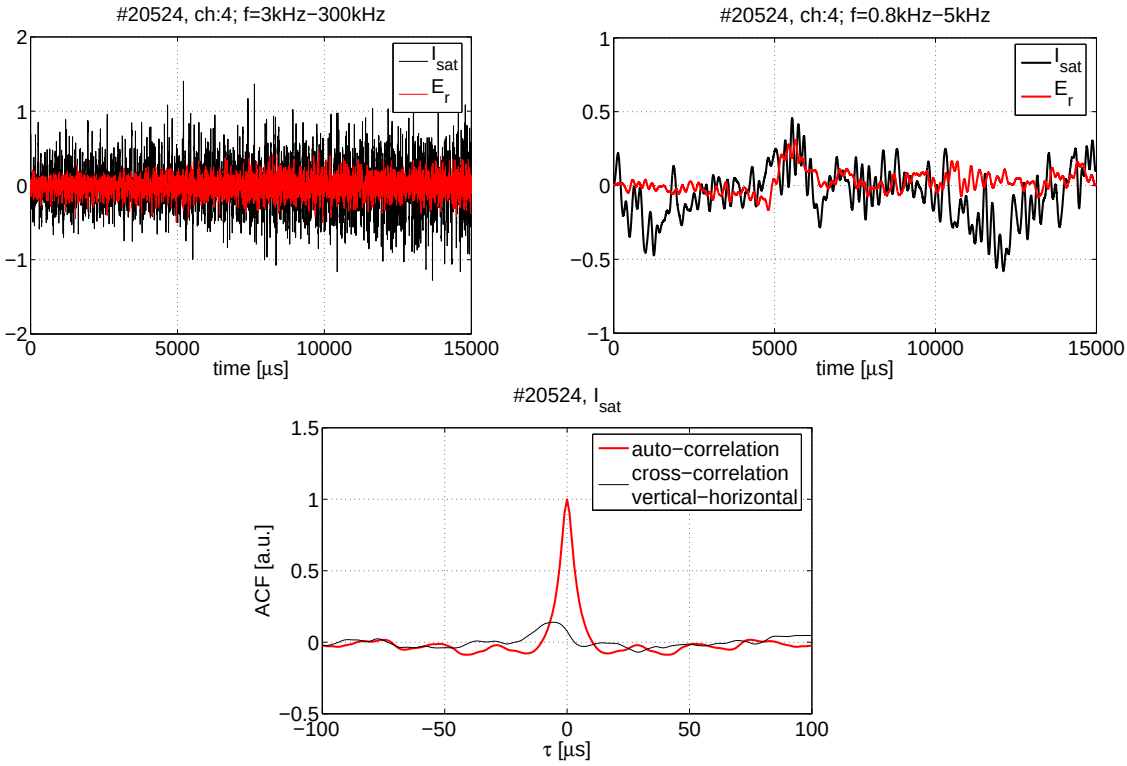

Figure 4.2: Raw signal for fast scale (left top) and for slow scale (right top). The auto-correlation and cross-correlation functions for the shorter time-scale (bottom).

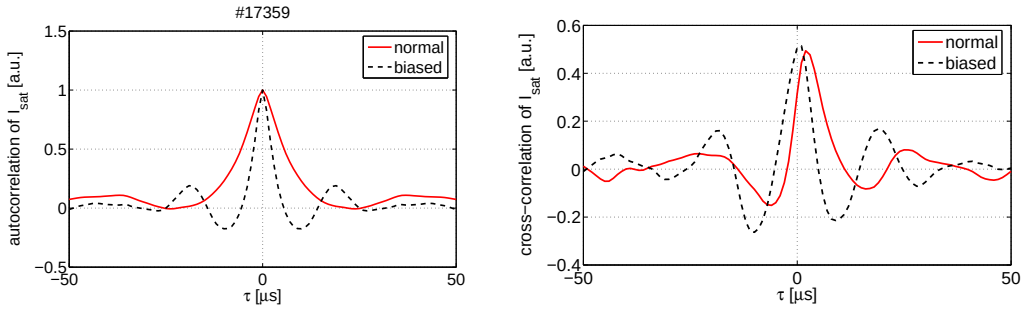

Figure 4.3: Comparison of one-point and two-point method in an real experiment

The temporal behaviour of the high frequency fluctuations of the plasma which are associated with the small scale plasma turbulence are shown in Fig. 4.4. The main coclusions ariseing from the fluctation measurements of floating potential ($\tilde{\Phi}_f$), ion saturation current ($\tilde{I}_{sat}$) and radial electric field ($\tilde{E}_r$) are the following: the characteristic time scale has been found to be about a couple of microseconds, $\approx 1cm$ radial correlation length has been detected and no direct correlation has been observed between the two poloidally 12 cm separated rake probes.

4.3 Correlation analysis of $W_{acf}(t)$

From direct measurement of the ion saturation current fluctuations we can estimate the autocorrelation function of the density fluctuations. The total fluctuating signal of about 15 ms – after an appropriate detrending procedure – was divided into $\Delta T = 75 - 100\mu s$ long sections. These are about 7 -10 times longer than the approximately 10 μs observed autocorrelation time.

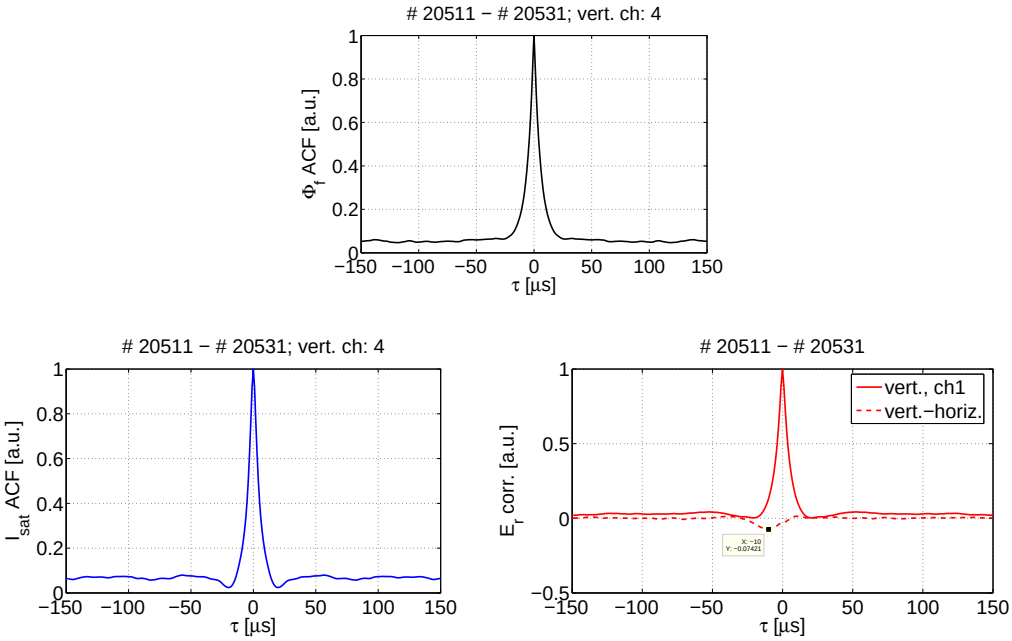

Figure 4.4: Characterization of basic turbulent structures

The $A_j(\tau)$ autocorrelation function was calculated for each section j. A single number, representing the width of the autocorrelation function in section j was calculated the following way:

$$w_j = \frac{\int_0^{\tau_0} \tau A_j(\tau) d\tau}{\int_0^{\tau_0} A_j(\tau) d\tau}, \quad \tau_0 = 10\mu s \tag{4.1}$$

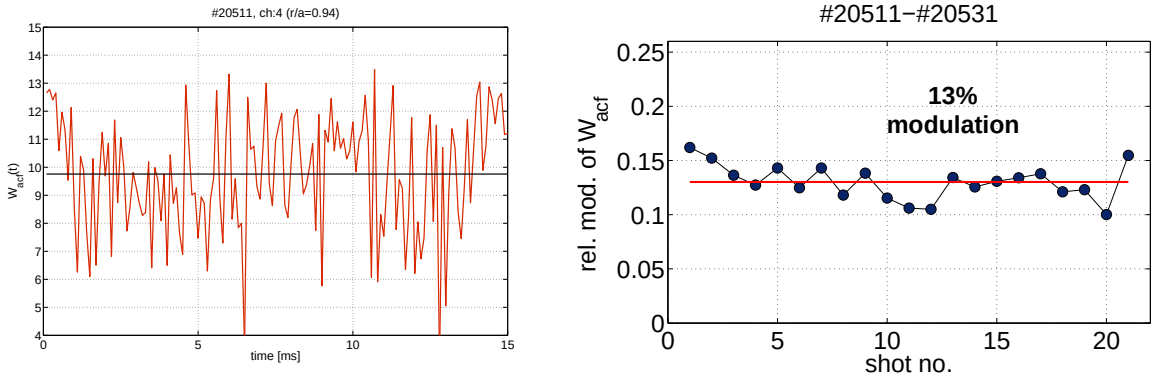

Figure 4.5: Time evolution of W_{acf} (left) and its relative modulation (right).

The time series of the $W_{acf}(t)$ plotted in Fig. 4.5 shows a relative modulation of about 13 % which is also the upper limit for the autocorrelation method (we refer to Eq. (3.9)). As it was mentioned above an ensemble of 'identical' shots has been made in order to improve statistics. The average over the ensemble of shots was done after calculating the correlation functions, and the effect is apparent in the bottom plots of Fig. 4.6, where an additional smoothig has also been done (red line).

After calculating ACF-width signals, $W_{acf}(t)$, for each ion saturation channel we proceed to calculate the detailed correlation structure of the $W_{acf}(t) \sim$ flow velocity modulations. The results are seen in Fig. 4.6. The left hand side of the figure shows the characteristic time scale of flow modulations (bottom)

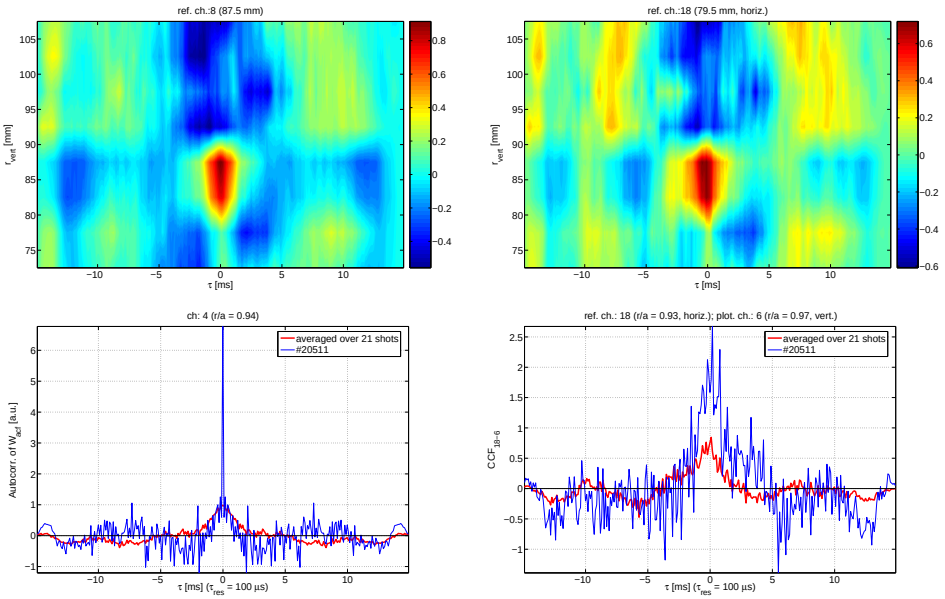

Figure 4.6: Space-time correlation structre of ZFs.

to be $\sim 1ms$, and the radial structure of the random flows (top) wich clearly indicates radial localization ($1cm$ width) in the edge plasma. Plots in the right hand side show the cross-correlation between a given reference channel located at the horizontal probe and all other channels at the vertical probe. On the basis of these calculations we can conclude that the flow structures remain significantly correlated in the poloidal direction even when measurement channels are separated by 12 cm which may be a signature of the high poloidal symmetry.

Before proceeding, it seems to be indispensable to check the possibility of misinterpretation of our results by an effect originatig from the global plasma changes rather than from relevant local features. To this end correlations between ACF-widths signal and relevant global parameters (U_{loop}, $X_{horizontal}$, $X_{vertical}$) have been determined. As it can be seen in Fig. 4.7 there are no correlated changes in the global plasma parameters and modulations in the flow velocity.

4.4 Connection of flow modulations to $\tilde{E}_r$ and $\tilde{n}_e$

Present experimental setup has allowed the measurement of radial electric field fluctuations and density fluctuations at the same radial position. Than it has become possible on the one hand to directly check the ACF-method correlating W_{acf} with $\tilde{E}_r$, (Fig. 4.8, left) and to explore connection between local density changes and flow modulations at the ZF time scales, correlating W_{acf} with $\tilde{I}_{sat}$, on the other hand (Fig. 4.8,right).

From the plots above it is clear that a connecton between flow fluctuations and the local changes of the density profile exists and causality relation also holds at the same milisecond timescale with the density changes leading the flow changes. It is also ovious that the statistics is rather poor as a cosequence of short time intervals for $W_{acf}(t)$.

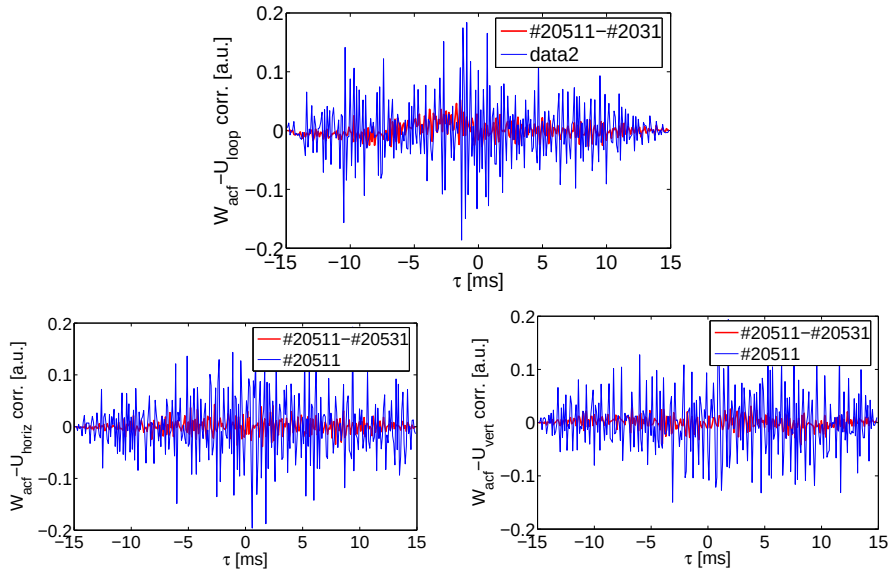

Figure 4.7: Correlations between W_{acf} signal and some global parameters.

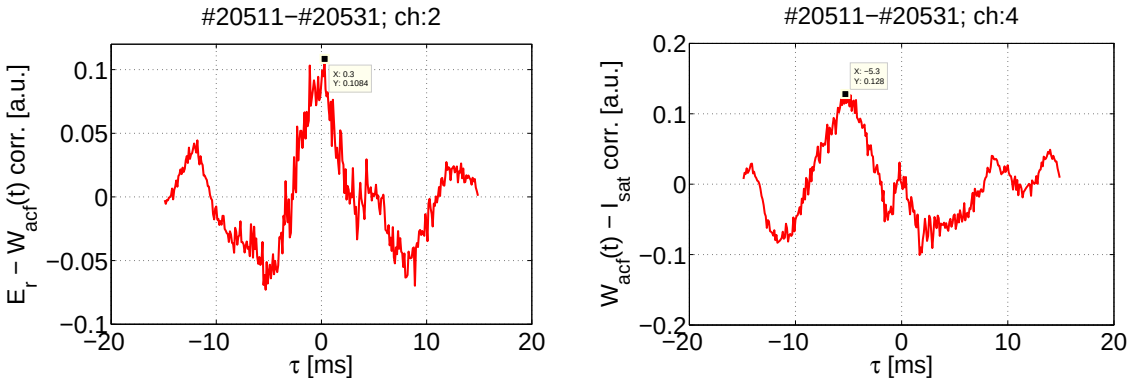

Figure 4.8: Cross-correlation of W_{acf} with $\tilde{E}_r$ (left) and $\tilde{n}_e$ (right)

Chapter 5

Conclusion

Detailed fluctuation measurements have been done in the Ohmic-heated discharges of the Castor tokamak. Density and radial electric field fluctuations have been detected using specially designed arrays of Langmuir probes, allowing radial-poloidal correlation measurements. The basic micro-turbulece has been characterized by means of autocorrelation functions along the rake probes. It has been found that the characteristc time scale and radial length of such structures lie in the domain of a couple of microseconds and a couple of centimeters respectively. It has been also demonstrated the applicability of the autocorrelation method in our case.

Autocorrelation-width analysis has been shown the existance of $\sim$ 13% rms modulations in the poloidal flow wich are radially well localized ($\sim 1cm$) and poloidally symmetric, having a characteristic lifetime of $\sim 1 - 2ms$. All these features strongly suggest the apparence of zonal flows described by theory as $m = 0, n = 0$ radially localized random potential structures. Our results are also consistent with the recent experimental work reported in [18]. In addition a possible connection between ZFs and local density profile changes (maybe connected with the turbulent transport) has also been found.

Bibliography

[1] A. Bencze, S. Zoletnik, Phys. Plasmas **12**, 052323, (2005).

[2] A. Yoshizawa, S. Itoh, K. Itoh and N. Yokoi, Plasma Phys. Control. Fusion **43**,$R1-R144$, (2001).

[3] P. H. Diamond,S. Itoh, K. Itoh and T. S. Hahm,Plasma Phys. Control. Fusion **47**,$R35-R161$, (2005).

[4] C. Holland, P. H. Diamond, S. Champeaux, E. Kim, et al., Nucl. Fusion, **43**, 761, (2003).

[5] A. M. Dimits et al., Phys. Plasmas **7**, 969, (2000).

[6] Z. Lin, T. S. Hahm, et al., Science **281**, 1835, (1998).

[7] B. N. Rogers, W. Dorland, and M. Kotschenreuther, **85**, 5336, (2000).

[8] C. Hidalgo, C. Silva, M. A. Pedrosa, E. Sanchez, H. Fernandes and C. A. F. Varandas, Phys. Rev. Lett. **83**, 2203, (1999).

[9] Y.H. Xu, C. X. Yu, J. R. Luo, J. S. Mao, B. H. Liu, J. G. Li, B. N. Wan, and Y. X. Wan, Phys. Rev. Lett. **84**, 3867, (2000).

[10] N. Vianello, E. Spada, V. Antoni, M. Sopolare, G. Serianni, G. Regnoli, R. Cavazzana, H. Bergsaker and J. R. Drake, Phys. Rev. Lett. **94**, 135001, (2005).

[11] C. Holland, G. R. Tynan, P. H. Diamond, R. A. Moyer and M. J. Burin,Plasma Phys. Control. Fusion **44**,$A453-A457$, (2002).

[12] R. A. Moyer,G. R. Tynan,C. Holland, and M. J. Burin, Phys. Rev. Lett. **87**, 135001, (2001).

[13] S. Coda, M. Porkolab, and K. H. Burell, Phys. Rev. Lett. **86**, 4835, (2001).

[14] M. Jakubowski, R. J. Fonck, and G. R. McKee, Phys. Rev. Lett. **89**, 265003,(2002).

[15] K. Hallatschek and D. Biskamp, Phys. Rev. Lett. **86**, 1223,(2001).

[16] G. D. Conway, B. Scott, J. Schirmer, M. Reich, A. Kendl and ASDEX Upgrade Team, 31st EPS Conf. on Contr. Fusion and Plasma Phys., London, 2004 **ECA 28G** $P-4.124$ (2004).

[17] G. S. Xu, B. N. Wan, M. Song, and J. Li, Phys. Rev. Lett. **91**, 125001, (2003).

[18] A. Fujisawa, K. Itoh, H. Iguchi, K. Matsuoka, S. Okamura, A. Shimizu, T. Minami, Y. Yoshimura, K. Nagaoka, C. Takahashi, M. Kojima, H. Nakano, S. Ohsima, S. Nishimura, M. Isobe, C. Suzuki, T. Akyama, K. Ida, K. Toi, S.-I. Itoh, and P. H. Diamond, Phys. Rev. Lett. **93**, 165002, (2005).